# Thalamocortical interactions shape hierarchical neural variability during stimulus perception

Adrià Tauste Campo[1*], Antonio Zainos[2], Yuriria Vázquez[2,a], Manuel Álvarez[2], Gustavo Deco[3,4], Ranulfo Romo[2,5,6*], Román Rossi-Pool[2,5*]

[1]Computational Biology and Complex Systems group, Department of Physics, Universitat Politècnica de Catalunya, Avinguda Dr. Marañón, 44-50, 08028 Barcelona, Catalonia, Spain

[2]Instituto de Fisiología Celular─Neurociencias, Universidad Nacional Autónoma de México, 04510 Mexico City, Mexico

[3]Center for Brain and Cognition (CBC), Department of Information Technologies and Communications (DTIC), Pompeu Fabra University, Edifici Mercè Rodoreda, Carrer Trias I Fargas 25-27, 08005, Barcelona, Catalonia, Spain

[4]Institució Institució Catalana de Recerca I Estudis Avançats (ICREA), Passeig Lluis Companys 23, 08010, Barcelona, Catalonia, Spain

[5]Centro de Ciencias de la Complejidad, Universidad Nacional Autónoma de México, Mexico City, Mexico.

[6]El Colegio Nacional, 06020 Mexico City, Mexico

[a]Present address: Laboratory of Neural Systems, The Rockefeller University, New York, NY 10065.

*Correspondence: adria.tauste@upc.edu (A.T.C.); ranulfo.romo@gmail.com (R.R.); romanr@ifc.unam.mx (R.R.-P.)

**The brain is hierarchically organized to process sensory signals. But, to what extent do functional connections within and across areas shape this hierarchical order? We addressed this problem in the thalamocortical network, while monkeys judged the presence or absence of a vibrotactile stimulus. We quantified the variability and a directed connectivity measure in simultaneously recorded neurons sharing the same cutaneous receptive field from the somatosensory thalamus (VPL) and areas 3b and 1 from the somatosensory cortex. During the stimulus presence, neuronal variability increased along the network VPL-3b-1. Furthermore, VPL and area 3b display fast dynamics with rapid feedforward interactions. In contrast, area 1 shows slower timescales with persistent intra-area interactions. Our results suggest that the lower variability of VPL and area 3b facilitates feedforward thalamocortical communication, while the higher variability of area 1 supports intra-cortical interactions during sensory processing. These results provide evidence of a hierarchical order along the thalamocortical network.**

## INTRODUCTION

Perception results from the interaction of neural networks that follow a hierarchical connectivity organization that extends from the receptors up to the cortex (1–3). The thalamus is known to play a key role in gating the flow of information to cortex (4). To unveil the intricacies of the thalamocortical network, several past studies have investigated the feedforward and feedback connections that link the thalamus and cortex (5–7). On this matter, a vast number of experimental studies on different sensory modalities (8–10) have provided a detailed model of the flow of sensory information processing in the thalamocortical network. This evidence has shown that it is composed of first order thalamic nuclei that act as sensory relay (feedback-driven) between the brainstem and the cortex, and of higher order nuclei that mediate cortico-cortical communications (4, 11, 12). In either case, thalamic nuclei have been shown to be drivers of cortical signals in contexts such as sensory representation (13, 14) and sensory adaptation (15, 16).

Over the last decades, the structural picture of the thalamocortical network has been refined thanks to functional connectivity studies on electrophysiological simultaneous recordings in both anesthetized (17) and awake animals (18, 19). Moreover, we have recently described the level of feedforward and feedback single-neuron functional

interactions between the ventral posterior lateral (VPL) nucleus of the thalamus and areas 3b and 1 of the primary somatosensory (S1) cortex during a vibrotactile detection task performed by trained monkeys (20). The results showed that feedforward prevailed over feedback interactions during stimulus perception and indicated the presence of zero-lag synchronization as a putative hallmark of active thalamocortical transmission. However, how these interactions were integrated into the hierarchical connectivity organization of the somatosensory network (21–24) remained unaddressed. In particular, it is unclear how functional connections in the thalamocortical network are constrained by the local properties of VPL (25, 26) and subareas 3b and 1 of S1 (27, 28). For instance, how are somatosensory interactions related to the capacity of neurons in each area to encode information? Are the interactions between VPL and each subarea of S1 different enough to support the relay role of area 3b? Or is VPL interacting analogously with neurons from areas 3b and 1? Further, are the intra and inter-area interaction affected by the response variability of the neurons (29–31)? Recently, the study of brain's hierarchical organization through the estimation of neural timescales (or time constants) has become a topic of intense research (21, 32–34). Specifically, the area's intrinsic timescale provides a quantification of the period in which the neurons of an area can integrate their input and is often associated to the strength of intra-area recurrent excitation (1). In this context, it is therefore natural to ask: how are functional interactions in the somatosensory network related to the capacity of the neurons to integrate inputs? In other words, are the intra-area interactions related to the intrinsic timescale of each network?

In the present study, we investigate the above questions by first measuring neural variability across two dimensions (inter-trial and intra-trial) as proxy to infer the distribution of Fano factors and timescales of each area and assess their concordance with areas hierarchical organization (1). Upon unravelling directed connections across VPL and areas 3b and 1, we report that VPL establish transient parallel feedforward connections with area 3b and area 1, respectively, that are concurrent to intra-area 1 connectivity, which is persistent over the entire stimulus period. While rapid feedforward connections are mainly supported by short timescale neurons from VPL and area 3b as well as small thalamic Fano factors, sustained intra-area 1 connectivity is supported by cortical neurons with high timescales. Thus, our refined analysis of thalamocortical functional connectivity (20) is shown to be integrated into the somatosensory hierarchical organization (23) reflecting a gradation along the pathway VPL-area 3b-area 1, by which

the individual variability of neurons from VPL and area 3b is particularly tuned to facilitate feedforward communication, while the variability of neurons from area 1 is aimed to supporting recurrent cortical connections. These results provide strong evidence that a hierarchical order in the somatosensory network could be established by employing variability measures, intrinsic timescales and directed information (DI) measures across the different areas of the thalamocortical network.

## RESULTS

To study the mutual influence between neural interactions and local firing rate variability, we analyzed the thalamocortical neuronal recordings obtained in two trained monkeys during a vibrotactile detection task in which the monkey received a mechanical vibration of variable amplitude and had to report whether the stimulus was present or absent by pressing a push button (Fig 1A, e.g. See (18, 25, 35) for details). Specifically, during those trials in which monkeys correctly performed the task, denominated as stimulus-present hits, or stimulus-absent correct rejections (Fig 1B), we analyzed the time-varying activity of neurons sharing receptive fields from the VPL nucleus (n=53 neurons) and S1 neurons (n=75; see Fig. 1C-D). Here, we classified the neuronal activity of S1 into two subareas: area 1 (n=60) and area 3b (n=15; Fig. 1C-D). First, we examined the mean firing rate in each population during stimulus-present (> 8 μm) hit trials and correct rejections (CR; Fig 1B). This firing-rate analysis revealed at least three main electrophysiological stages for supra-threshold stimuli (Fig 1E, top), while the responses during CRs maintained a consistent differentiation between the three areas (Fig. 1E, bottom). Specifically, during the first half of the stimulus period (0-0.25s), area 1 showed larger firing rates than the converging values of area 3 and VPL. Note that during the second half of the stimulus (0.25-0.5s), the firing rate of the three areas decreased to a similar average value. The latency distributions in each area (Fig. 1F) highlighted the shift tendency observed across the somatosensory processing: VPL-3b-1.

To unravel the link between neural variability and thalamocortical interactions during stimulus perception, we explored two sources of spiking variability. 1) Within-trial temporal variability, measured by the autocorrelation decay parameter known as the *intrinsic timescale* (32). 2) Inter-trial variability, measured by the *Fano factor*, evaluated across trials recorded during a fixed experimental condition. We next characterize the neuronal activity of each area according to both sources of variability.

### Intrinsic timescales exhibit a thalamocortical hierarchical organization

To infer the intrinsic timescales of the recorded populations in VPL, area 3b and area 1, we followed (32) and more recent works (33, 34). The timescale constant studied for this purpose was the exponential decay rate of the basal (resting state or foreperiod) autocorrelation. We focused on the spontaneous spiking activity of each unit during a common fixed period of 1.5s before stimulation onset. We separately estimated the intrinsic timescale for single neurons and for each area (Methods). In both cases, we calculated and fit the corresponding autocorrelation function (either one per neuron or one per area) via an exponential function with $\tau$ parameter equal to the intrinsic timescale. First, to obtain a $\tau$ for each neuron separately, we constructed the autocorrelation function by averaging accumulated autocorrelation values across time bin pairs of the same temporal distance. Then, to estimate densities, we only considered the neurons that showed sufficient convergence guarantees in the parameter fitting solution (Methods). When inspecting the timescale distribution in each area (Fig. 2A), the broader distribution of area 1 in contrast to VPL suggested a larger diversity of autocorrelation decay rates in this sensory cortex than in the thalamus. Furthermore, the intrinsic timescale was significantly smaller in VPL than in area 1 (VPL, median $\tau$ = 9.5ms; area 1, median $\tau$ = 15.9ms, Ranksum test, $P<0.05$). Moreover, neurons in area 3b were positioned in between (median $\tau$ = 11.8ms) showing closer values to VPL timescales.

On the other hand, to obtain intrinsic timescales at the population level, we constructed a single autocorrelation function per area by averaging pooled values across neurons and time bin pairs. The parameter-fitting results obtained with this second approach (Fig. 2B-D) were shown to be stable for VPL ($\tau$ = 9.8ms, Fig. 2B) while they were slightly shifted to greater values for area 3b ($\tau$ = 14.1ms, Fig 2C) and area 1 ($\tau$ = 17.2ms, Fig 2D). Taken together, these results exhibited the same hierarchical ordering than the median timescales obtained from single-neuron distributions, reflecting how the timescale becomes longer across somatosensory network. In particular, the resulting timescales suggest a larger level of integration of the S1 as compared to the VPL in agreement with previous results obtained in the rodent visual pathway (34). These findings also pinpoint the existence of specific neural dynamics associated to different regions (area 3b, area 1) within S1.

**The Fano factor correlates with the hierarchical somatosensory network**

To complement the previous analysis, we also examined the inter-trial variability inherent to each area, estimating the Fano factor of each neuron across correct trials (Fig 3,

Methods). The Fano factor measures the overdispersion of a given multiple-trial sample with respect to the Poisson distribution under a fixed experimental condition (29–31, 36). Importantly, it has been recently discussed that the practical estimation of the Fano factor can be largely biased by neuronal firing rate fluctuations (31, 37) and its applications on spiking datasets exhibiting super-Poisson variability during stimulus presence is questionable (30). Nevertheless, previous studies, have employed this metric to establish a hierarchy across the visual pathway (38), to differentiate different network states (39) or to exhibit a widespread mechanism to decrease variability across the cortex (36).

Here, we averaged the Fano factor across each stimulus-amplitude value to obtain a single value per neuron and plot its variation during the time course of stimulus-present trials in each area (Fig 3A). A visual inspection of the dynamic plots in Fig 3A suggested that both the baseline average value and the stimulus-driven decline increased across the hierarchy. To quantify the Fano factor decline at stimulus onset, we computed the area under the receiver operating characteristic curve (AUROC, or in short, AUC) between the distributions of Fano at each task interval and the obtained from the basal period. The results showed that AUC was significantly lower during the stimulus period in the three areas (Fig 3B, VPL, AUC=0.41, $P < 0.01$; area 3b, AUC=0.38 $P < 0.05$; area 1, AUC=0.31, $P < 0.01$). Again, this Fano factor decline established a hierarchical processing across the somatosensory network.

To further analyze this decline during the stimulus period, we examined the mean-to-variance spike-count relationship (Fig. 3C). A visual inspection of these plots suggested the existence of a sublinear dependence between variance and mean firing rate in VPL and a supralinear dependence in area 1 (30). Then, we pooled the Fano Factor for neurons from each area to compute their distributions (Fig. 3D). Importantly, the median of each distribution ($F_{\mathrm{VPL}}$=0.79; $F_{\mathrm{Area\ 3b}}$=1.01; $F_{\mathrm{Area\ 1}}$=1.19) showed again a hierarchical ordering across the three areas ($F_{\mathrm{VPL}}<F_{\mathrm{Area\ 3b}}<F_{\mathrm{Area\ 1}}$). Overall, these results demonstrate that the stimulus-driven inter-trial variability also reflects a hierarchical ordering, showing that area 3b neurons lay in between the sub- and supra-Poisson distributions associated with VPL and area 1, respectively.

Afterwards, we examined the relation between the intrinsic timescale and the Fano factor during stimulus-present trials (Fig S1) for VPL and area 1. Note that both metrics (τ and Fano) exhibit a correlation during the basal period. Remarkably, the traces shown deviate (Fig. S1A) during the stimulus period (0-0.5s, Fig S1B, VPL, $\rho = 0.52$; area 1, $\rho =$

0.21). Then, only in area 1, correlation between variability and intrinsic times diminish during stimulation, providing evidence that both sources of variability become uncoupled as the sensory information is projected from the thalamus to S1.

**Parallel thalamocortical interactions between VPL-area 3b and VPL-area 1.**

To estimate the directed information interactions across the studied areas during correctly detected trials (0-5s), we employed a methodology developed in previous works (20, 40). Briefly, we used a non-parametric method that measures the directed coupling between the simultaneously recorded spike trains of pairs of neurons in single trials and within slicing time windows of 0.25m. The method is illustrated in Fig. 4A. We first estimated delayed versions of the directed information-theoretic measure in both directions for every pair of neurons at the short time delays [0,2,4,…,20 ms]. To infer the significance of each estimation, we defined a maximizing-delay statistic and built the corresponding null distribution (Fig. 4A, middle). For each directional spike-train pair, the method assessed the significance of the statistic together with an unbiased estimation of the statistic value and the maximizing-delay (Fig. 4A, right). Spike-train pairs associated with significant estimators ($\alpha$=0.05) are referred as Directional Information (DI) trials and will be represented for different experimental conditions as a percentage over the corresponding pairs and trials.

When studying DI for pairs of spike trains belonging to different areas along the somatosensory network VPL-3b-1, we assume that feedforward interactions are composed of VPL→area 3b, VPL→area 1, area 3b→area 1. Analogously, we assume that feedback interactions are composed of area 1→area 3b, area 1→VPL, area 3b→VPL. Motivated by previous findings (20), we only considered bidirectional zero-lag DI (or in short, zero-lag synchronization) among all possible bidirectional combinations. These types of interactions are mounted by instantaneously coupled spike trains, that is, spike trains that are coupled in both possible directions at a delay of 0 ms. For the sake of clarity, Fig. 4B shows a schematic representation for the three types of interactions.

The estimation of interactions across inter-area pairs in VPL-3b-1 (Fig 4C) revealed that feedforward DI (blue curves) prevailed over feedback DI (red curves) during the stimulus period for both VPL-area 3b and VPL-area 1. In general, DI percentage after the stimulus period did not differ from pre-stimulus values, suggesting a stimulus-driven DI modulation in these areas. In both cases, the percentage of DI after stimulus onset (0-

0.25s) significantly increased with respect to pre-stimulus values (VPL→area 3b, $H = 0.23$, $P < 0.01$; VPL→area 1, $H = 0.25$, $P < 0.01$). Thus, directional information is comparable between VPL-area 3b and VPL-area 1. So, even if a hierarchical ordering could be established across these areas, the thalamic influence appears to be akin. Remarkably, for pairs area 3b-area 1, feedback was much strongly manifested than feedforward interactions (Fig. 4C, left and middle). The variation of feedback DI during the stimulus period ($H = 0.25$, $P < 0.01$) contrasts with the moderate increase in feedforward DI after stimulus onset ($H = 0.13$, $P < 0.05$). Then, contrary to expected, stimulus-driven interaction between area 3b and 1 was mainly feedback (Fig. 4C, right).

The curves shown in Fig 4C correspond to supra-threshold trials ($A > 9\mu m$). Analogous results were found for other amplitudes, demonstrating the stability of the reported results (Fig. S2). In addition, the stimulus-driven nature of the described results was supported by the replication of Fig 4C during correct rejected trials (Fig. S3). Indeed, Fig. S3A shows that there were no significant DI variations with respect to the baseline period during neither the possible stimulation window (41) nor any posterior task interval. Moreover, to assess whether the previous results were biased by the main observation of VPL-area 3b-area 1 through independent recording sessions, we restricted the results of Fig 4C to the experimental sessions in which VPL, area 3b and area 1 were simultaneously recorded (Fig S4). Supporting our previous results, feedforward DI showed a significant stimulus-driven increase (VPL→area 3b, $H = 0.18$, $P < 0.01$; VPL→area 1, $H = 0.18$, $P < 0.01$).

Given that feedforward DI from VPL is analogous between area 3b and 1, it suggests that area 3b is not playing a relay role in broadcasting the sensory information that arrived from VPL towards area 1. To further test this conjecture, we analyzed the feedforward DI delays associated to each inter-area (Fig S5). Importantly, the histograms displayed in Fig S5C showed that the feedforward average delay between VPL and area 1 ($\widehat{D} = 9.6$ ms) was incompatible with the addition of feedforward VPL→area 3b ($\widehat{D} = 7.1$ ms) and area 3b→area 1 ($\widehat{D} = 7.2$ ms). This result does not support the relay role hypothesis for area 3b. Further, it agrees with Fig. 4C (right) that shows that interaction between areas 3b and 1 is mainly feedback, during the last part of the stimulus. Then, information appears to be streamed in parallel pathways from VPL to areas 3b and 1.

Finally, we analyzed the dynamics of inter-area zero-lag synchronization over the time course of the task (Fig 4C, orange). This coupling was shown previously to be a relevant feature for effective vibrotactile stimulus detection (20). Our results demonstrate that synchronization appeared more prominently between VPL and area 3b ($H = 0.25$, $P < 0.01$) than between VPL and area 1 ($H = 0.14$, $P < 0.01$). Note that, zero-lag coupling between areas 3b and 1 is not modulated throughout the task. This interaction across areas may play a mechanistic role in the transmission and stability of sensory information from VPL to S1 (20).

**Stimulus-driven intra-area interactions in area 1.**

Afterwards, we focus on the interaction within each area (VPL, 3b and 1). In this case, DI estimations could be of two types: 1) unidirectional interactions, in which spike-trains from the same area were coupled in one out of the two possible directions; 2) bidirectional zero-lag synchronization, when spike trains were coupled in both directions at zero delay. Fig. 4D shows a schematic representation for both types of interactions. Fig. 4E show the percentage of DI within each area across supra-threshold trials (Fig 4E). We found that the arrival of stimulus elicited a pronounced unidirectional intra-area DI in area 1 ($H = 0.21$, $P < 0.01$) and a much more modest interaction in area 3b ($H = 0.12$, $P < 0.01$). Importantly, the increase in DI within area 1 was preserved during the whole stimulus period, in contrast with the decay observed in VPL→area 1 feedforward DI (Fig. 4C, middle). As for bidirectional zero-lag synchronization, area 1 replicates the temporal trace of unidirectional interactions with a sustained increase over the entire stimulus period ($H = 0.18$, $P < 0.01$). We replicated these results for stimulus-absent trials (Fig S3B) to manifest the stimulus-driven effect observed in Fig. 4E.

In conclusion, the above results suggest different roles for the intra-area interactions across these areas. Our data shows that upon stimulus arrival, VPL establishes comparable stimulus-driven feedforward DI to both somatosensory areas, area 3b rapidly synchronizes with VPL (VPL↔area 3b) to strengthen these interactions. However, area 1 concurrently exhibits local connectivity (area 1→area 1) that is sustained during the entire stimulus presentation. Therefore, area 1 is equipped with longer timescale, higher variability and displays stronger intra-area stimulus-driven interactions, essential features to integrate, transform and maintain sensory information.

**Correlations between Fano factor and thalamocortical interactions.**

In this section, we quantify the interplay between local variability measures and thalamocortical interactions. First, we computed the association between the Fano factor (Fig 3A) and the inter-area feedforward DI during the stimulus period. To perform such analysis, we separately considered VPL→area 3b (Fig. 5A left), and VPL→area 1 (Fig. 5A right). Then, for both DI, we estimated the correlation across neurons between the average Fano factor throughout the task and its corresponding outgoing (VPL→) or incoming (→area 3b, →area 1) DI rates. For each neuron, we computed this DI rates as the percentage of feedforward DI across all stimulus-present trials and involved pairs (Methods). Fig. 5A (left) shows the results for VPL→area 3b, exhibiting a putative link between the Fano factor and the DI rate per neuron. Note that VPL and area 3b exhibit opposite values of correlation; when feedforward DI increases, variability diminishes in VPL but increments in area 3b. Indeed, a stronger negative correlation was found for VPL during stimulation ($\rho$=-0.55, $P$<0.1) and a positive one for area 3b ($\rho$=0.68, $P$<0.01). Importantly, the analysis of VPL→area 1 further supported the negative correlation between feedforward DI and VPL Fano factor (Fig 5A right). Fig. 5B shows the corresponding scatter plot during the first half of the stimulus period ($\rho$=-0.51, $P$<0.01). Notably, the incoming feedforward DI to area 1 was totally uncoupled from the inter-trial variability throughout the entire task (Fig 5A right, $P$>0.1). Therefore, while feedforward DI correlates positively with Fano in area 3b and negatively in VPL, it appears uncorrelated to variability in area 1.

The above results suggested a relation between the firing rate variability of VPL neurons and their feedforward associations with neurons from the S1. In more general terms, it meant that the less variable the neurons of VPL were across trials, the more prone they were to establish significant interactions with S1. Therefore, more reliable neurons in VPL (low Fano factor) tend to create significant directional information interactions with S1. However, neurons from area 3b showed a different trend. Specifically, area 3b neurons with significant feedforward DI with VPL tended to increase their inter-trial variability upon stimulus arrival (0.25-0.5 s). On the contrary, the firing rate variability of neurons in area 1 was unaffected by the incoming information from VPL, suggesting that the influence of feedforward inputs into the internal dynamics of area 1 was modest.

To further illustrate the distinct associations Fano factor with feedforward DI, in Fig 5C and 5D we divided neurons from each area into two groups (low [dark] and high [light] Fano factor neurons) according to the area's median Fano factor during stimulation. Fig.

5C shows that this division of neurons separated low and high Fano factor neurons throughout the entire task, which demonstrated that variability is a representative feature of each neuron. Afterwards, in Fig 5D we computed the percentage of feedforward DI from VPL (Fig. 5D left) to area 3b (Fig. 5D middle) and to area 1 (Fig. 5D right), for low and high Fano factor neurons. Indeed, Fig. 5D further illustrates that both, the low variability group in VPL and the high variability group in area 3b, yielded larger feedforward DI (Fig. 5D left, $P < 0.001$; Fig. 5D middle, $P < 0.1$, significant trend). In contrast, no directional information differences across groups were observed in area 1. Taken together, these findings report that variability may play a relevant role for establishing feedforward DI in VPL and area 3b, but this effect vanishes in area 1.

**Correlations between intrinsic timescales and inter and intra-area interactions.**

Subsequently, we study the relationship between thalamocortical DI and each area's intrinsic timescale (Fig 2). Unlike the Fano factor, the timescale was estimated once, during the pre-stimulus period. In this section, we included in the analysis the interaction between VPL and the whole S1 (VPL→S1). Analogous to Fig. 5, we estimated the association across neurons' timescales and its feedforward DI. We divided neurons from each area into two groups (low [dark] and high [light] $\tau$ neurons) according to each neuron's timescale with respect to the area's median value. For each group, we plotted the percentage of feedforward DI from VPL (Fig. 6A, left); to area 3b (Fig. 6B, left); and to area 1 (Fig. 6C, left). Importantly, neurons from VPL and area 3b with the lowest $\tau$ displayed higher percentage of feedforward DI (Fig. 6A, left, VPL, $P < 0.01$; Fig. 6B, left, area 3b, $P < 0.05$). Notably, the timescales from neurons in area 1 did not play a significant role regarding the incoming feedforward DI (Fig. 6C, left).

Finally, we extended this analysis to the intra-area results. We split the neurons according to their timescale and for each group we computed the percentages of intra-area DI for VPL (Fig. 6A, right), area 3b (Fig. 6B, right), and area 1 (Fig. 6C, right). The results demonstrate that area 1 neurons with highest timescale were significantly more prone to integrate inter-area interaction during the entire stimulus period (Fig. 6C, right, $P < 0.01$). Moreover, the influence of timescale on intra-area DI is much more modest in VPL (Fig. 6A, right) and area 3b (Fig. 6B, right). These finding support modelling works that establish a relation between intrinsic timescales and intra-area recurrent interactions (1). In conclusion, the study of the relationship between intrinsic timescales and directional information unveils that the main reported interactions trends found in this study,

feedforward DI and sustained intra-area 1 DI, were facilitated, respectively, by low timescale ranges in VPL and area 3b and high timescale ranges in area 1. This shows again a differentiated hierarchical role of each area along the somatosensory network.

## DISCUSSION

In brief, we show strong evidence that a hierarchical order in the somatosensory network could be established by employing variability measures, intrinsic timescales and directed information (DI) measures across the different areas of the thalamocortical network. Although these measures quantify different aspects of the network dynamics, a hierarchical picture (1) could be established through the coordination of all of them. Furthermore, complementary, and interlinked aspects of the network infrastructure could also be obtained from these different measures. Therefore, this work establishes a relationship between these metrics, generating thus, a comprehensive picture of the roles of the different components of the network.

While time constants may play a relevant functional role to determine the period over which areas integrate their inputs (1, 21, 32), inter-area DI represent the degree of recurrent interplay. Here, we provide evidence that relates the timescales with recurrent interactions. As it is known, brain circuits require a diversification of recurrent connectivity and timescales during perceptual processes (42). Under this requirement, long time constants and strong recurrent interaction may promote the sensory transformation that depends on signal integration or its maintenance. However, long time constants, strong variability, and inter-area information flow, could be an impediment when generating a precise representation of the stimulus. Then, networks with more modest recurrent interaction are still necessary. This might yield a connection between functional and structural heterogeneities.

Based on previous anatomical evidence, VPL is viewed as a first-order relay nucleus (11), where somatosensory information is conveyed mainly to areas 3b and 1. Our results provide further evidence to support this idea by showing that the intra-area information flow within VPL is not modulated. Then, in contrast to areas 3b and 1, recurrent processing (intra-area interactions) is not modulated during the sensory input within VPL. In agreement with this result, autocorrelation decay is much smaller in VPL than S1, indicating a modest reverberation. Moreover, VPL shows smaller firing rate variability than both subareas of S1. Further, VPL neurons with smaller Fano Factor, tend to communicate more information to cortical neurons, which means that the VPL tendency

to display a small variability, is related with its main goal, to transmit reliable information to the cortical somatosensory network.

Historically, VPL and S1 were considered as sensory areas, mainly implicated in pure phase locking responses (3, 43, 44). Additionally, areas 3b and 1 were both considered as part of S1, with analogous responses and few or nonclear differences between them (45, 46). Further, recent anatomical evidence has suggested that both areas show akin amounts of synaptic projected from VPL (47). Here, we confirmed that during the perceptual detection of the vibrotactile stimulus, the amount of incoming feedforward interactions during the stimulus period is comparable in area 3b and area 1. Additionally, contrary to the hypothesis that propose as area 3b as a relay to area 1, feedforward interactions during stimulation were poorly modulated. Notably, feedback DI (3b←1) were the most prominent interactions between these areas. Then, even if discrepancies in the variability, intra-area interactions and timescales were found between these areas, they are not established by differences in VPL inputs. One possible hypothesis is that they emerge as a consequence of structural differences in these networks (1). In relation with this conjecture, we identified a functional difference between these areas. Whereas area 3b is more engaged in receiving inputs from VPL with small recurrent information flow, area 1 yields much higher variability, time constant and recurrent interactions. This means that one area is more equipped to represent VPL inputs, while the other to process and to integrate somatosensory information that has already reached the cortex. Moreover, while area 3b variability and autocorrelation decay are related to the VPL inputs, these same measures in area 1 are not modulated by the incoming VPL feedforward DI. This is further evidence that each area deals differently with VPL information, such that they have separated sub-specializations.

Although recording in isolated neurons exhibit stochastic variability, they appear much more stable than recording from brain areas (48). Then, a portion of the variability occurs from variations in the synaptic currents of each network (29, 30). Previous studies have suggested that such degree of variability at a single-neuron level increases with the stages of sensory processing, being lowest in the periphery and highest in cortical structures (30, 34, 38). Importantly, VPL, areas 3b and 1 displayed hierarchical differences between their variabilities resting state and stimulation period. Notably, area 1 shows the highest variability during the basal period and the strongest decrease during the stimulation period. Additionally, during this period, the area 1 single cell timescales decorrelate with

their inter-trial variability and increase the relation with the intra-area interactions. Moreover, the intra-area feedforward input from VPL does not correlate with the area 1 variability. These findings exhibit dynamics differences between these areas. While variability in VPL and area 3b are affected by feedforward interactions, inputs to area 1 are diluted by network processing.

It is important to emphasize that our analytical approach employs nonparametric significance tests to compute the percentage of significant DI to estimate the interaction between and across areas (49). Previous studies have shown that DI has a weak dependence with the firing rate of neurons. Instead, it estimates the interaction across neurons in a quasi-orthogonal dimension to the neural activity. Therefore, DI quantifies, in a single trial and for any given time, how much information can be obtained from the recent past and present spike train of a given neuron about the present spike train of another, simultaneously recorded neuron. Finally, we remark that our results rely on a correlation analysis between functional interactions estimated a single-trial level (and averaged across trials) and variability measures estimated at a multiple-trial level, thus adding additional robustness to potential sample biases.

One important question for future research is how oscillation signals like the local field potentials (LFP) are affected by variability, timescales, and local and inter-area interactions. Is it possible to observe these differences in hierarchy looking at the inter and intra-area oscillatory coherence? Furthermore, future experiments involving multi electrodes recording are essential to clarify the role of the different cortical layers (50). Are there any differences in variability and time constant across each cortical column? How do the intra, feedforward and feedback information flow change across the different cortical layers? Is it possible to establish a hierarchy of processing across these layers?

To conclude, we would like to point out that the synergy between feedforward and feedback interactions and inherent dynamical features like the ones computed here, shape the function of each brain network. Diversification of structural and dynamics features among cortical and subcortical networks, may be central to discerning brain function and computations during cognitive processes.

**ACKNOWLEDGMENTS**

We thank to Yuriria Vázquez for her contribution during the experiments. We thank Hector Diaz for his technical assistance. A.T.C was supported by the Spanish national research project (ref. PID2020-119072RA-I00 /AEI/10.13039/501100011033) funded by the Spanish Ministry of

Science, Innovation, and Universities (MCIU) and by the Bial Foundation grant 106/18. G.D. was supported by the Spanish national research project (ref. PID2019-105772GB-I00 /AEI/10.13039/501100011033) funded by the Spanish Ministry of Science, Innovation, and Universities (MCIU). This work was supported by grants PAPIIT-IN205022 (to R.R.-P.) from the Dirección de Asuntos del Personal Académico de la Universidad Nacional Autónoma de México and CONACYT-319347 (to R.R.-P.) and CB2014-20140892 (to R.R.) from Consejo Nacional de Ciencia y Tecnología.

## METHODS

### Detection task

The detection task and neural recordings follow along the same lines as (20, 25, 51). Vibrotactile stimuli were delivered to the skin of the distal segment of one digit of the restrained hand, via a computer-controlled stimulator (BME Systems, MD; 2-mm round tip). The initial probe indentation was 500 µm. Vibrotactile stimuli consisted of trains of 20 Hz mechanical sinusoids (20 ms duration), with amplitudes of 1-34 µm (Fig. 1A). These were interleaved with an equal number of trials where no mechanical vibrations were delivered to the skin (amplitude = 0). A trial began when the probe tip (PD) indented the skin of one fingertip of the restrained, right hand, upon which the monkey placed its free, left hand on an immovable key (KD). After a variable pre-stimulus period (1.5-3 s), a vibrotactile stimulus could be presented or not (0.5 s). Note that the possible period of stimulation lasts 1.5s longer than the stimulus, as can be seen in the differences in shadow areas in Fig. 1E (top) and Fig. 1E (bottom). After a fixed delay period (3 s), the stimulator probe was lifted off from the skin (PU), indicating to the monkey that it could initiate the response movement (KU) to one of two buttons (PB). The button pressed indicated whether the monkey felt the stimulus (henceforth referred as 'yes' and 'no' responses, respectively). They were rewarded with a drop of liquid for correct responses. Psychometric detection curves were obtained by plotting the proportion of 'yes' responses as a function of the stimulus amplitude (left panel of Fig. 1B). Depending on whether the stimulus was present or absent and on the behavioral response, the trial outcome was classified as hit, miss, false alarm or correct rejection (right pane of Fig. 1B). Monkeys were handled according to the institutional standards of the National Institutes of Health and Society for Neuroscience. All protocols were approved by the Institutional Animal Care and Use Committee of the Instituto de Fisiología Celular of the National Autonomous University of Mexico (UNAM).

**Recordings**

Neuronal recordings were obtained by using two arrays, each with seven independent, movable microelectrodes (1.3 −3 MΩ; (25, 51)). One array was inserted into S1 (cyan spot on the figurine of left panel of Fig. 1C), in the cutaneous representation of the fingers (areas 1 or 3b; middle panel of Fig. 1C). The other array was located lateral and posterior to the hand's representation (green spot on the left panel of Fig. 1C) of the Ventral Posterior Lateral thalamus (VPL). We located the microelectrodes in the cutaneous representation of the fingers in the VPL. Recordings were performed contralateral to the stimulated hand (right) and ipsilateral to the responding hand (left). Each recording began with a mapping session to find the cutaneous representation of the fingers in VPL. Subsequently, we mapped neurons in S1 sharing receptive fields with the neurons of VPL (Fig. 1D). All recorded neurons had small cutaneous receptive fields with quickly (QA, VPL: n = 65, S1: n=71) or slowly adapting (SA, VPL: n = 9, S1: n=4) properties. Locations of the electrode penetrations in VPL and S1 were confirmed with standard histological techniques. Additionally, neurons from S1 were classified into areas 1 (n=60) and 3b (n=15). The neuronal signal of each microelectrode was sampled at 30 kHz and spikes were sorted online. A more extensive description of the task and recording procedure can be found in previous publications (25, 51). Here, we report data from multiple recording sessions during which spikes were obtained. For the experimental condition, we recorded 47 sessions with 120−140 trials per session (53 neurons in VPL, 75 neurons in S1, 84 VPL-S1 pairs). All activity is aligned to the minimum duration of the variable period, 1.5s before stimulus onset.

**Intrinsic timescales estimation**

We computed the intrinsic timescales following the same method described in (32, 33) applied at single neuron level. Let us first model the time-binned spike counts of a spike train as a doubly stochastic process in which each time bin is of duration Δ. Then, the autocorrelation *R(.)*, being a function of the time lag $k\Delta$ *(k=1,2,…)* between pairs of time bins indexed by their onset times $i\Delta$ and $j\Delta$ ($k=|i-j|$), can be approximated by the exponential decay function:

$$R(k\Delta) = A\left(e^{-\frac{k\Delta}{\tau}} + B\right) , \qquad \text{[eq. 1]}$$

where $A$ is a multiplying constant, $\tau$ is the decay rate constant measuring the intrinsic timescale, and $B$ accounts for the contribution of timescales longer than the observed windows.

We computed the autocorrelation function $R(.)$ in our datasets along similar lines of previous works (32–34). First, from every single spike train, we obtained a spike-count time series binned in steps of $\Delta ms$ and windows widths of $W_b\, ms$ during a baseline period of 1.5s following the KU event and prior to stimulus onset. Then, in every neuron, for each pair of bins ($i\Delta$ and $j\Delta$, $i,j=1,2,\ldots,i\neq j$) we computed the Pearson correlation between the spike count values at bins $i\Delta$ and $j\Delta$, respectively, over all recorded trials. Finally, to obtain the autocorrelation function $R(k\Delta)$, Pearson correlation coefficient values were accumulated and averaged over at each time bin difference $k\Delta$ $(k=|i-j|)$. The maximum time difference is $D_{max}=k_{max}\,\Delta$. To obtain the above autocorrelation function for every single neuron, we accumulated and averaged the correlation coefficient over all time bin pairs at each time bin difference $k\Delta$. Then, the autocorrelation functions were fit by the exponential decay function [eq. 1] using nonlinear least-squares fitting via the Levenberg-Marquardt algorithm. For each brain area under study, we only selected neurons whose fitting outcome was sufficiently good base on either the fitted parameters converged to a solution, or the residual difference was less than a specified tolerance ($10^{-6}$) over a maximum number of iterations ($500$). In the following we call these neurons *well-fitted neurons*. As a result, we obtained an estimation of the intrinsic timescale $\tau$ per well-fitted neuron.

To obtain an autocorrelation function at the population level, we accumulated correlation coefficient estimates over all time bin pairs and well-fitted neurons within an area, averaging them at each time bin difference $k\Delta$. After undergoing the fitting procedure, we obtained an estimation of the intrinsic timescale $\tau$ per area. In parallel, to assess the robustness of this estimation, we computed the autocorrelation matrix for each well-fitted neuron separately and averaged the matrices across neurons. Then, we defined the autocorrelation function at each time bin difference $k\Delta$ by averaging the coefficient estimates over the corresponding time bin pairs in this matrix. This alternative method yielded approximately the same quantitative results, thus validating the initial estimation.

In agreement with a previous works (33), we applied the above procedures with steps of $\Delta=20ms$, windows widths of $W_b=40ms$, and maximum time difference of $D_{max}=500ms$. The results did not change qualitatively for variations ±10% of $\Delta$ and $W_b$. In our dataset,

the percentage of well-fitted neurons per area were 58% in VPL (n=31), 60% in area 3b (n=9), and 88% in area 1 (n=53). Finally, confidence intervals for the intrinsic timescales were estimated using non-parametric bootstrapping (52).

**Fano factor estimation**

Let *N(w)* be a counting process describing the number of spikes in a time interval *(0,w)*, of length *w>0*, in which the time zero is conventionally set a priori. The Fano factor is a measure of the variability of *N(w)* defined as the variance to mean ratio of the number of spikes in a time window of a length *w* (30, 31, 37):

$$F(w) = \frac{\mathrm{Var}\left(N(w)\right)}{E\left(N(w)\right)}, w > 0 \qquad \text{[eq. 2]}$$

The Poisson process is an example of a counting process for which the above variance-to-mean ratio equals one. Since Poisson processes have traditionally been a popular model to model stimulus-evoked spike counts (29), the Fano factor has been employed in many studies to characterize the degree of overdispersion of the observed neural firing rate with respect to the Poisson distribution. Hence, in practice, a Fano factor significantly larger or smaller than 1 is an indicator that the variability of the observed counting process is larger or smaller than the variability of a Poisson process, respectively.

In practice, the Fano factor for a single neuron in a limited time window is estimated based on *n* independent observed spike counts during repeated trials of a fixed experimental condition (e.g., trials in which a vibrotactile stimulus of the same amplitude is delivered). The standard estimator of the Fano factor is then based on the ratio of unbiased estimators of the variance and mean of the *n* spike counts (see for instance (31), eq. 20). In our study, for every neuron and task interval of 250 ms, we estimated the Fano factor over *n* hit trials at a fixed amplitude and averaged the Fano factor estimates across amplitude values. For each Fano factor estimation, we selected *n* to be equal or larger than 5 trials. We removed Fano factor estimates lying *3* standard deviations above and below the median value prior to perform the stimulus-amplitude average. On the other hand, during stimulus-absent trials, we estimated the Fano Factor from correctly rejected trials (*n≥5*). Hence, during both conditions (hit and correct rejected trials), we obtained one Fano factor estimate per neuron and task interval.

Although the Fano factor has been popularly used in many neuroscience studies (36, 38, 39, 53), recent works have showed that the estimation of the *F(w)* might be influenced by

the neuronal firing rate and advocate for unbiased definitions of neural variability (30, 31, 37). However, in our study we obtained one variability measure per neuron, and the resulting values only showed a significant dependence on the mean firing rate in VPL, which was of negative sign and temporally localized outside the stimulus period. Consequently, we discarded introducing any firing-rate correction in the analysis.

**Single Directed Information (DI) estimation**

The method used to estimate directional interactions at a single-trial level was described in detail in (20, 40). The software to perform such estimations is available as a package ("DI-Inference") in both Matlab (https://github.com/AdTau/DI-Inference) and Python (https://github.com/mvilavidal/DI-Inference-for-Python) languages. The package includes an exemplary script with simple simulated toy models to evaluate the method's performance (54).

**Feedforward, feedback information and zero-lag interactions**

As in (20), when studying DI interactions for two simultaneous spike trains at a given time interval (e.g., 0.25 s) one may consider three disjoint cases: the spike trains are coupled in only one direction, in only the opposite direction or simultaneously coupled in both directions. In principle, these three cases correspond to neurons in each pair taking three different roles: driver, target, or both. According to this notion, we classified DI estimates per trial by pairing the role (driver, target) of each neuron with its location according to the presumed directionality of the somatosensory pathway VPL →area 3b→area 1. In short, we defined as feedforward information the DI estimates obtained from genuine driver-target pairs (VPL, area 3b; VPL→ area 3b), (VPL, area 1; VPL→ area 1), and (area 3b, area 1; area 3b → area 1). Similarly, we defined as feedback information the ones obtained from the genuine driver-target pairs (area 3b, VPL; area 3b → VPL), (area 1, VPL; area 1→VPL), and (area 1, area 3b; area 1 → area 3b). Finally, pairs where both neurons were simultaneously drivers and targets at zero delay were labelled as zero-lag interactions.

**Statistical analysis: Quantification of significant effects on DI percentages**

The main metric used in Fig. 4 was obtained by aggregating each DI type (feedforward, feedback, and zero-lag interactions) over all neuron pairs and trials at individual task intervals and computing their percentage over the total amount of trials. Specifically, the stimulus-driven change in the percentage of DI illustrated in Fig. 4, was tested as an

unpaired comparison using a non-parametric test for correlated samples (55) relying on Cohen's effect size (Cohen's H; (56)) statistic, which measures the distance between two proportions $p_1$ and $p_2$ as:

$$H^{unpaired}(p_1, p_2) = 2\left(arcsin\sqrt{p_1} - arcsin\sqrt{p_2}\right) \quad \text{[Eq. 3]}$$

The use of this statistic allows to straightforwardly quantify the size of any significant effect by comparing its value with standardized thresholds (H = 0.2, small effect size; H = 0.5, medium effect size; H = 0.8 large effect size), thus avoiding sample size biases. Non-parametric tests for correlated samples were performed through 1000 group-based permutations (55) where groups were defined to be single trials and group sample sizes were maintained in each permutation. Thus, our analysis avoided introducing any statistical bias to the sampled reference distribution.

**Correlation of Fano factor and intrinsic timescales with percentage of DI**

To assess the potential association between spike-train directionality across pairs of somatosensory areas and local neuronal variability, we correlated the percentage of the DI with the intrinsic timescale and the average Fano factor across all neurons of each area using Spearman's rank-order correlation ($\rho$). In this analysis, we mainly focus on the percentage of feedforward information during the first half of the stimulus period (0-250ms). This choice was made because feedforward information was shown to be largely modulated by the stimulus presence in real data and the DI in general was shown to be sufficiently robust to additive noise at the firing rates of the stimulus period in simulated models (See (20), Fig. S5). To compute the correlation ($\rho$), we obtained one directionality value per neuron by averaging the percentage of DI over its recorded pairwise interactions. By doing so, we avoided introducing repeated measures per neuron in the analysis.

For both, the intrinsic timescales and the Fano factor computed during the stimulus interval, we correlated the corresponding variability metric ($\tau$ or *Fano*) obtained for every single neuron with the percentage of incoming/outgoing feedforward information. We particularized the above analysis within each area (VPL, area 3b and area 1) leading to three distinct computations: the correlation of $\tau$/*Fano* with the percentage of (outgoing) VPL-S1 feedforward information across VPL neurons; the correlation of $\tau$/*Fano* with the percentage of (incoming) VPL-Area 3b feedforward information across area 3b neurons,

and the correlation of *τ/Fano* with the percentage of (incoming) VPL-area 1 feedforward information across area 1 neurons.

**REFERENCES**


1. X.-J. Wang, Macroscopic gradients of synaptic excitation and inhibition in the neocortex. *Nat. Rev. Neurosci.* **21**, 169–178 (2020).

2. J. A. Harris, *et al.*, Hierarchical organization of cortical and thalamic connectivity. *Nature* **575**, 195–202 (2019).

3. R. Romo, R. Rossi-Pool, Turning Touch into Perception. *Neuron* **105**, 16–33 (2020).

4. S. M. Sherman, R. W. Guillery, The role of the thalamus in the flow of information to the cortex. *Philos. Trans. R. Soc. London. Ser. B, Biol. Sci.* **357**, 1695–1708 (2002).

5. M. M. Halassa, S. M. Sherman, Thalamocortical Circuit Motifs: A General Framework. *Neuron* **103**, 762–770 (2019).

6. G. M. G. Shepherd, N. Yamawaki, Untangling the cortico-thalamo-cortical loop: cellular pieces of a knotty circuit puzzle. *Nat. Rev. Neurosci.* **22**, 389–406 (2021).

7. C. O'Reilly, E. Iavarone, J. Yi, S. L. Hill, Rodent somatosensory thalamocortical circuitry: Neurons, synapses, and connectivity. *Neurosci. Biobehav. Rev.* **126**, 213–235 (2021).

8. H. J. Alitto, W. M. Usrey, Corticothalamic feedback and sensory processing. *Curr. Opin. Neurobiol.* **13**, 440–445 (2003).

9. S. R. Crandall, S. J. Cruikshank, B. W. Connors, A Corticothalamic Switch: Controlling the Thalamus with Dynamic Synapses. *Neuron* **86**, 768–782 (2015).

10. F. Briggs, W. M. Usrey, Corticogeniculate feedback and visual processing in the primate. *J. Physiol.* **589**, 33–40 (2011).

11. S. M. Sherman, Thalamus plays a central role in ongoing cortical functioning. *Nat. Neurosci.* **19**, 533–541 (2016).

12. S. M. Sherman, The thalamus is more than just a relay. *Curr. Opin. Neurobiol.* **17**, 417–422 (2007).

13. K. Reinhold, A. D. Lien, M. Scanziani, Distinct recurrent versus afferent

dynamics in cortical visual processing. *Nat. Neurosci.* **18**, 1789–1797 (2015).

14. J. Yu, D. A. Gutnisky, S. A. Hires, K. Svoboda, Layer 4 fast-spiking interneurons filter thalamocortical signals during active somatosensation. *Nat. Neurosci.* **19**, 1647–1657 (2016).

15. C. J. Whitmire, Y. J. Liew, G. B. Stanley, Thalamic state influences timing precision in the thalamocortical circuit. *J. Neurophysiol.* **125**, 1833–1850 (2021).

16. N. C. Wright, *et al.*, Rapid Cortical Adaptation and the Role of Thalamic Synchrony during Wakefulness. *J. Neurosci.* **41**, 5421 LP – 5439 (2021).

17. R. M. Bruno, B. Sakmann, Cortex is driven by weak but synchronously active thalamocortical synapses. *Science* **312**, 1622–1627 (2006).

18. S. Haegens, *et al.*, Thalamocortical rhythms during a vibrotactile detection task. *PNAS* **111**, E1797-805 (2014).

19. A. M. Bastos, F. Briggs, H. J. Alitto, G. R. Mangun, W. M. Usrey, Simultaneous recordings from the primary visual cortex and lateral geniculate nucleus reveal rhythmic interactions and a cortical source for γ-band oscillations. *J. Neurosci. Off. J. Soc. Neurosci.* **34**, 7639–7644 (2014).

20. A. Tauste Campo, *et al.*, Feed-forward information and zero-lag synchronization in the sensory thalamocortical circuit are modulated during stimulus perception. *PNAS* **116**, 7513–7522 (2019).

21. R. Chaudhuri, K. Knoblauch, M.-A. Gariel, H. Kennedy, X.-J. Wang, A Large-Scale Circuit Mechanism for Hierarchical Dynamical Processing in the Primate Cortex. *Neuron* **88**, 419–431 (2015).

22. M. Ashaber, *et al.*, Connectivity of somatosensory cortical area 1 forms an anatomical substrate for the emergence of multifinger receptive fields and complex feature selectivity in the squirrel monkey (Saimiri sciureus). *J. Comp. Neurol.* **522**, 1769–1785 (2014).

23. N. Saadon-Grosman, S. Arzy, Y. Loewenstein, Hierarchical cortical gradients in somatosensory processing. *Neuroimage* **222**, 117257 (2020).

24. Y. Song, *et al.*, Feedforward and feedback pathways of nociceptive and tactile processing in human somatosensory system: A study of dynamic causal modeling

of fMRI data. *Neuroimage* **234**, 117957 (2021).

25. Y. Vázquez, E. Salinas, R. Romo, Transformation of the neural code for tactile detection from thalamus to cortex. *PNAS* **110**, E2635–E2644 (2013).

26. W. Song, M. Semework, Tactile representation in somatosensory thalamus (VPL) and cortex (S1) of awake primate and the plasticity induced by VPL neuroprosthetic stimulation. *Brain Res.* **1625**, 301–313 (2015).

27. J. H. Kaas, R. J. Nelson, M. Sur, C.-S. Lin, M. Merzenich, Multiple Representations of the Body Within the Primary Somatosensory Cortex of Primates. *Science* **204**, 521–523 (1979).

28. M. Sur, J. T. Wall, J. H. Kaas, Modular distribution of neurons with slowly adapting and rapidly adapting responses in area 3b of somatosensory cortex in monkeys. *J. Neurophysiol.* **51**, 724–744 (1984).

29. E. P. Simoncelli, L. Paninski, J. Pillow, O. Schwartz, Characterization of neural responses with stochastic stimuli. *Cogn. Neurosci.* **3**, 1 (2004).

30. R. L. T. Goris, J. A. Movshon, E. P. Simoncelli, Partitioning neuronal variability. *Nat. Neurosci.* **17**, 858–865 (2014).

31. K. Rajdl, P. Lansky, L. Kostal, Fano Factor: A Potentially Useful Information . *Front. Comput. Neurosci.* **14**, 100 (2020).

32. J. D. Murray, *et al.*, A hierarchy of intrinsic timescales across primate cortex. *Nat. Neurosci.* **17**, 1661–1663 (2014).

33. R. Rossi-Pool, *et al.*, Invariant timescale hierarchy across the cortical somatosensory network. *PNAS* **118**, e2021843118 (2021).

34. J. H. Siegle, *et al.*, Survey of spiking in the mouse visual system reveals functional hierarchy. *Nature* (2021) https:/doi.org/10.1038/s41586-020-03171-x.

35. V. de Lafuente, R. Romo, Neuronal correlates of subjective sensory experience. *Nat. Neurosci.* **8**, 1698–1703 (2005).

36. M. M. Churchland, *et al.*, Stimulus onset quenches neural variability: a widespread cortical phenomenon. *Nat. Neurosci.* **13**, 369–378 (2010).

37. A. S. Charles, M. Park, J. P. Weller, G. D. Horwitz, J. W. Pillow, Dethroning the Fano Factor: A Flexible, Model-Based Approach to Partitioning Neural

Variability. *Neural Comput.* **30**, 1012–1045 (2018).

38. P. Kara, P. Reinagel, R. C. Reid, Low response variability in simultaneously recorded retinal, thalamic, and cortical neurons. *Neuron* **27**, 635–646 (2000).

39. A. S. Ecker, *et al.*, State Dependence of Noise Correlations in Macaque Primary Visual Cortex. *Neuron* **82**, 235–248 (2014).

40. A. Tauste Campo, *et al.*, Task-driven intra- and interarea communications in primate cerebral cortex. *PNAS* **112**, 4761 LP – 4766 (2015).

41. F. Carnevale, V. de Lafuente, R. Romo, O. Barak, N. Parga, Dynamic Control of Response Criterion in Premotor Cortex during Perceptual Detection under Temporal Uncertainty. *Neuron* **86**, 1067–1077 (2015).

42. M. R. Joglekar, J. F. Mejias, G. R. Yang, X.-J. Wang, Inter-areal Balanced Amplification Enhances Signal Propagation in a Large-Scale Circuit Model of the Primate Cortex. *Neuron* **98**, 222-234.e8 (2018).

43. R. Luna, A. Hernández, C. D. Brody, R. Romo, Neural codes for perceptual discrimination in primary somatosensory cortex. *Nat. Neurosci.* **8**, 1210–1219 (2005).

44. V. B. Mountcastle, M. A. Steinmetz, R. Romo, Frequency discrimination in the sense of flutter: psychophysical measurements correlated with postcentral events in behaving monkeys. *J. Neurosci.* **10**, 3032–3044 (1990).

45. V. de Lafuente, R. Romo, Neural correlate of subjective sensory experience gradually builds up across cortical areas. *PNAS* **103**, 14266–14271 (2006).

46. E. Salinas, A. Hernández, A. Zainos, R. Romo, Periodicity and Firing Rate As Candidate Neural Codes for the Frequency of Vibrotactile Stimuli. *J. Neurosci.* **20**, 5503–5515 (2000).

47. Y. Mir, *et al.*, Modular Organization of Signal Transmission in Primate Somatosensory Cortex. *Front. Neuroanat.* **16** (2022).

48. Z. F. Mainen, T. J. Seinowski, Reliability of spike timing in neocortical neurons. *Science* **268**, 1503–1506 (1995).

49. M. Gilson, A. Tauste Campo, X. Chen, A. Thiele, G. Deco, Nonparametric test for connectivity detection in multivariate autoregressive networks and application

to multiunit activity data. *Netw. Neurosci.* **1**, 357–380 (2017).

50. N. A. Steinmetz, *et al.*, Neuropixels 2.0: A miniaturized high-density probe for stable, long-term brain recordings. *Science* **372**, eabf4588 (2021).

51. Y. Vázquez, A. Zainos, M. Alvarez, E. Salinas, R. Romo, Neural coding and perceptual detection in the primate somatosensory thalamus. *PNAS* **109**, 15006–15011 (2012).

52. P. I. Good, *Permutation, parametric and bootstrap tests of hypotheses* (Springer Science & Business Media, 2005).

53. M. N. Shadlen, W. T. Newsome, The Variable Discharge of Cortical Neurons: Implications for Connectivity, Computation, and Information Coding. *J. Neurosci.* **18**, 3870 LP – 3896 (1998).

54. AdTau, AdTau/DI-Inference v1.0. *Zenodo* (2020) https:/doi.org/10.5281/ZENODO.4059445 (August 2, 2021).

55. A. M. Winkler, G. R. Ridgway, M. A. Webster, S. M. Smith, T. E. Nichols, Permutation inference for the general linear model. *Neuroimage* **92**, 381–397 (2014).

56. J. Cohen, *Statistical power analysis for the behavioral sciences* (Academic press, 2013).

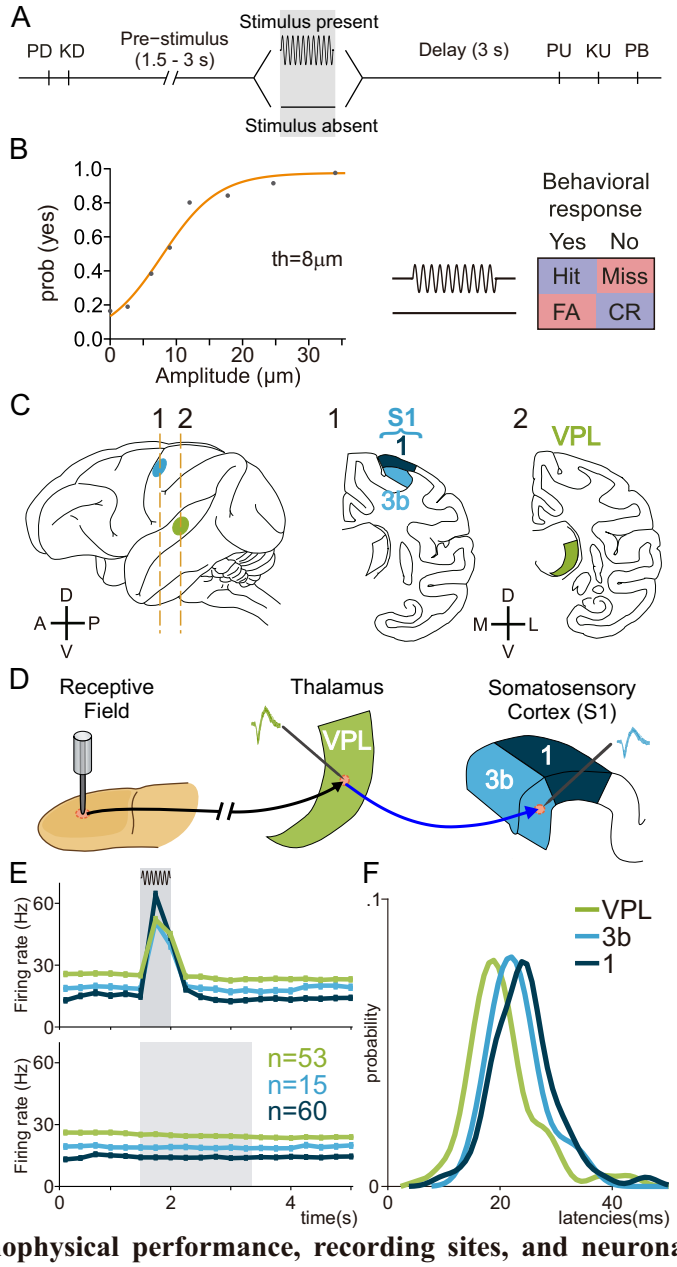


**Figure 1: Detection task, psychophysical performance, recording sites, and neuronal responses during the task**. (A) Vibrotactile detection task. Trials began when the stimulator probe indented the skin of one fingertip of the monkey's restrained right hand (probe down, PD); the monkey reacted by placing its left, free hand on an immovable key (key down, KD). After a variable prestimulus period (1.5 to 3 s), a vibratory stimulus of variable amplitude (1 to 34 μm, 20 Hz, 0.5-s duration) was presented on one half of the trials; no stimulus was presented on the other half of the trials. Following the stimulus presentation period (whether the stimulus was present or not), the monkey waited for 3 s until the probe was lifted off from the skin (PU, probe up), then the animal releases the key (KU, key up) and pressed one of two push buttons (PBs) to report whether the stimulus was present (lateral button) or absent (medial button). Stimulus-present and stimulus-absent trials were randomly interleaved within a run. (B, Left) Mean psychometric function depicting the probability of the monkey's reporting yes (presence) as a function of the stimulus amplitude (th = 8 μm, detection threshold). (B, Right) Behavioral responses depending on the stimulus presence (Hit or Miss) or stimulus absence (CR, correct rejection; FA, false alarm). (C) Recording sites in the thalamus ventral posterior lateral (VPL) nucleus (green) and in areas 1 (dark blue) and 3b (light blue) of the primary somatosensory cortex (S1). (D) Scheme depicting how the neural activity from single neurons in the VPL and S1 (3b or area 1) sharing the same cutaneous receptive field was simultaneously recorded during the detection task. (E) Mean firing rate for the simultaneously recorded VPL (n = 53), Area 3b (n = 15) and Area 1 (n=60) neurons supra-threshold hits (top) and correct rejections (CR, bottom). The timescale is aligned to the minimum variable period, 1.5s before stimulus onset. Grey rectangle (top) represents stimulation period, while grey rectangle (bottom) represents the possible period of stimulation, according to task design. Note the differences during the first (0-0.25s) and second (0.25-0.5s) stimulus period responses during hits. (F) Probability density of the neuronal response latencies with respect to stimulus onset during hit trials.

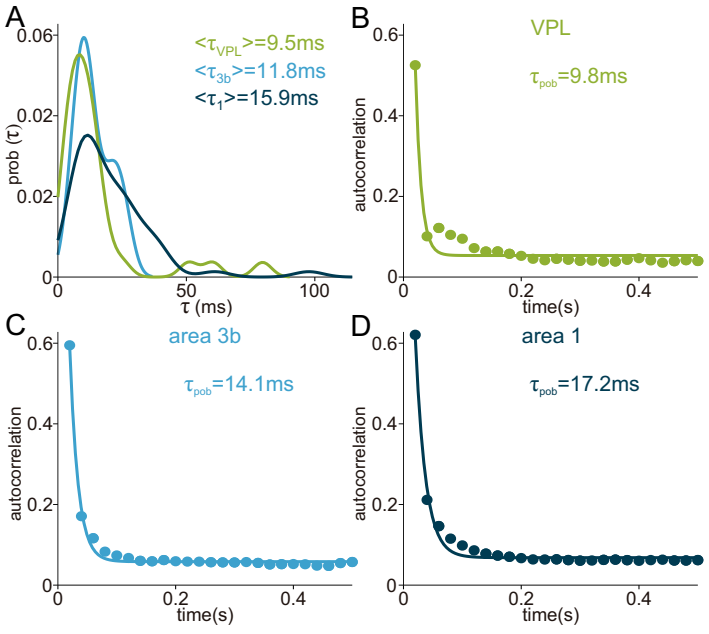


**Figure 2: Areas' intrinsic timescales are hierarchically ordered across the somatosensory network.** Autocorrelation functions were computed on the spiking activity recorded during the basal period (1.5s) before stimulus onset. An exponential decay function was fit to the resulting autocorrelation function. Confidence intervals for the decay rate parameter intrinsic timescale (τ) were estimated through non-parametric bootstrap. (A) Distribution of neuronal τ in each area (green, VPL, n=31, median τ=9.5±2ms; light blue, area 3b, n=9, median τ=11.8±2ms; dark blue, area 1, n=53, median τ=15.9±2ms. (B-D) Population autocorrelation and fitted exponential decay function by each area. Colored filled dots represent the average autocorrelation values for each time bin difference (across pairs and neurons). Solid lines represent the fitted exponential decay function. (B) VPL (green, n=31 neurons, τ=9.5±3ms). (C) Area 3b (light blue, n=9 neurons, τ=14.1±3ms). (D) Area 1 (dark blue, n=53 neurons, τ=17.2±1ms).

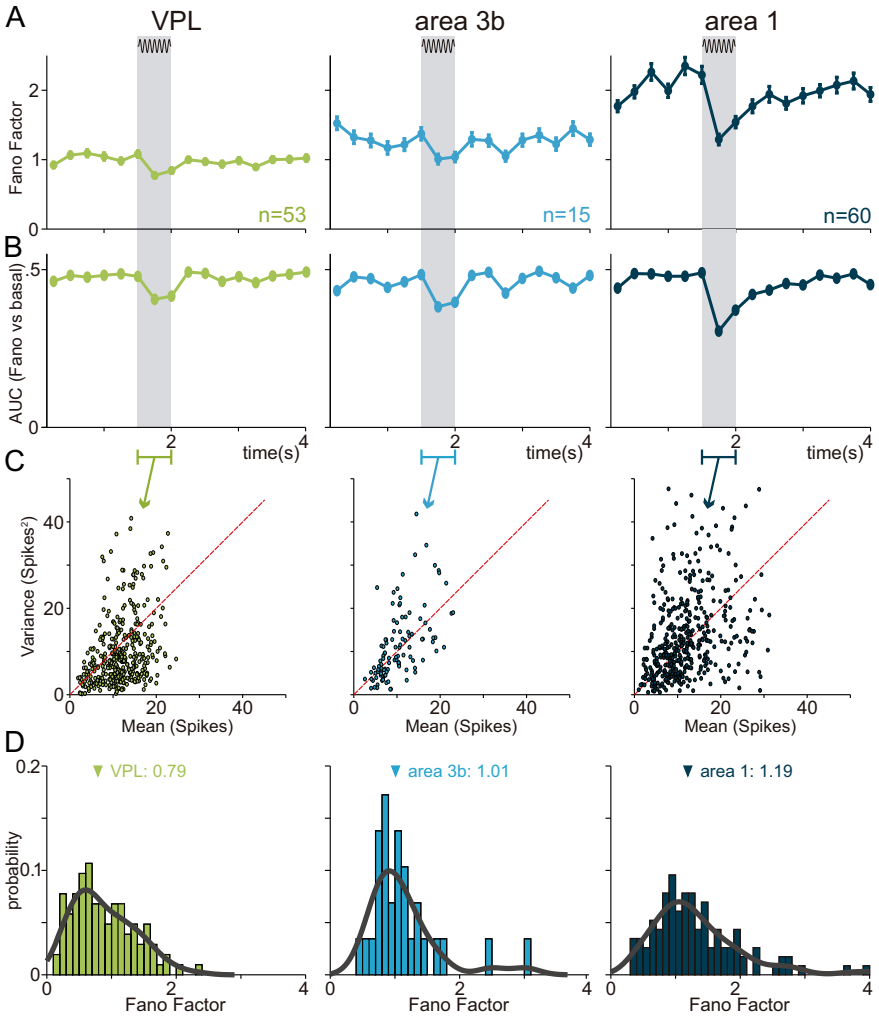


**Figure 3: Fano factor is hierarchically distributed across the somatosensory pathway.** (A) Time-varying average Fano factor during hit trials for each area (VPL, n=53 neurons; area 3b, n=15 neurons; area 1, n=60 neurons). Values for each neuron are computed and averaged over all amplitudes with sufficient number of hit trials (≤5). Error bars denote the SEM with respect to the mean over neurons in each area. Shaded area highlights the stimulus period. (B) AUC computed between the Fano factor baseline distribution and each interval distribution for each area. Lower values with respect to 0.5 mean larger statistical differences between both distributions at each task interval. AUC were significantly lower during the stimulus period in the three areas (VPL, AUC=0.41, $p<0.01$; area 3b, AUC=0.38 $p<0.05$; area 1, AUC=0.31, $p<0.01$). (C) Relationship between the average and the variance of the number of spikes during stimulus period intervals. Each dot corresponds to a different stimulus amplitude for each neuron (VPL, n=406; area 3b, n=112; area 1, n=448). The red dashed line plots the identity straight line (mean=variance) that should follow a Poisson distribution. (D) Histograms and estimated probability density of Fano factor per neurons during the stimulus period (VPL, n=103; area 3b, n=29; area 1, n=115). Medians are indicated on top of each plot ($F_{VPL}$=0.79; $F_{Area3b}$=1.01; $F_{Area1}$=1.19).

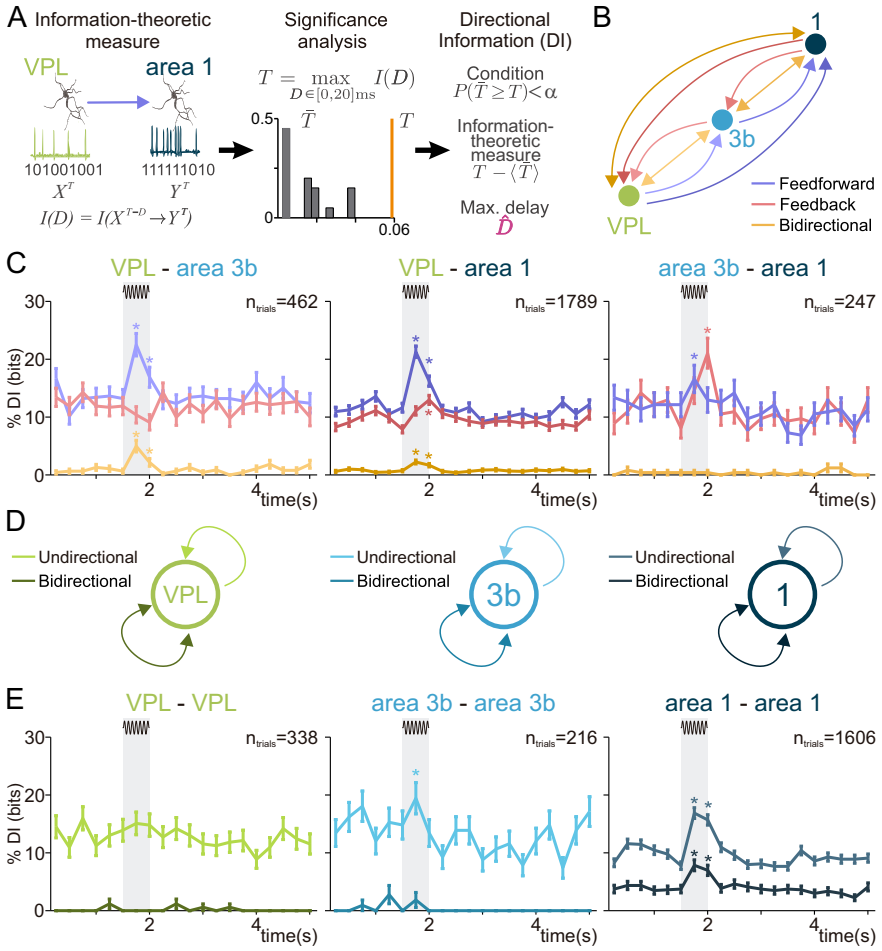


**Figure 4: Inter and intra-area directional interactions in the thalamocortical network.** (A) Sequential scheme representing the method to infer DI at single trial level. Left: information-theoretic measure is estimated between single-trial spike trains of the simultaneously recorded neurons in VPL and area 1 for delays (0,2,4, ⋯ ,20) ms. Middle: significance is locally determined via non-parametric testing ($\alpha=0.05$) of a maximizing-delay statistic. Right: every significant trial ($P<\alpha$) is denoted as Directional Information (DI) trial and is associated with an unbiased value and a delay. (B) Scheme showing feedforward, feedback and bidirectional interactions across VPL, area 3b and area 1. The arrows connecting VPL and area 1 are slightly darker colors to indicate the relationships in (C). Darker colors represent direct interactions without passing through area 3b as an intermediary. (C) Percentage of DI trials for feedforward (blue), feedback (red) and bidirectional zero-lag (orange) interactions are shown along the task during supra-threshold hits. Left: VPL-area 3b neuron pairs (n=462 trials). Middle: VPL-area 1 pairs (n=1789 trials). Right: area 3b-area 1 pairs (n=247 trials). Error bars denote the SEM. Asterisks denote significant differences ($P < 0.05$) between a pre-stimulus baseline (1s) and stimulus periods. H (Cohen's H) measures the effect size of each DI type: VPL→area 3b, H=0.23; VPL↔area 3b, H=0.25; VPL→area 1, H=0.25; VPL↔area 1, H=0.14 ($P < 0.01$). Shaded area highlights the stimulus period (500 ms). (D) Scheme showing unidirectional and bidirectional interactions within VPL (left), area 3b (middle) and area 1 (right). (E) Percentage of DI trials for unidirectional (lighter color) and bidirectional zero-lag interactions (darker color) are shown throughout the task during supra-threshold hit trials. Left: VPL-VPL pairs (n=338 trials). Middle: area 3b-area 3b pairs (n=216 trials). Right: area 1-area 1 pairs (n=1606 trials). H (Cohen's H) for each DI type during stimulation: area 3b→area 3b, H=0.12; area 1→area 1, H=0.21; area 1↔area 1, H=0.18 ($P < 0.01$).

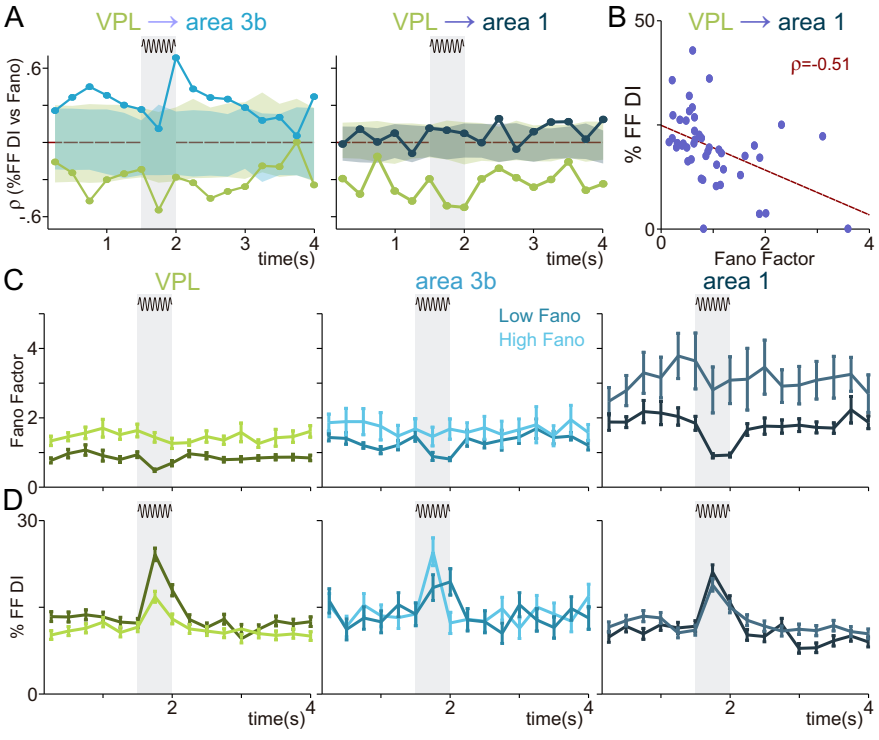


**Figure 5: Feedforward interactions are differentially linked to Fano Factor in each area.** (A) Spearman's rho correlation ($\rho$) between the time-varying Fano factor in thalamocortical pair (VPL-area 3b, VPL-area 1) and their respective feedforward DI during the stimulus period (0-0.25s). The horizontal shaded area shows one standard deviation above and below the average surrogate value (in dashed). Left: Correlations ($\rho$) in VPL (green, n=12) and area 3b (light blue, n=15). Right: Correlations ($\rho$) in VPL (green, n=45) and area 1 (dark blue, n=60). (B) Scatter plot showing the negative correlation ($\rho$) between the VPL Fano factor and feedforward VPL→area 1 DI from VPL to area 1 during the stimulus period (0-0.25s, $\rho$=-0.51, $P<0.01$). (C) Average Fano factor during the task in VPL (left), area 3b (middle) and area 1 (right) as a function of two groups of neurons (low [dark-colored] and high [light] Fano factor neurons). These groups are split by the population median during the stimulus**.** (D) Percentage of feedforward information from VPL (left), to area 3b (middle) and to area 1 (right), during the task (0-4s) for the two groups of neurons. Error bars denote the SEM. In (C) and (D) shaded areas highlight the stimulus period (0-0.5 s).

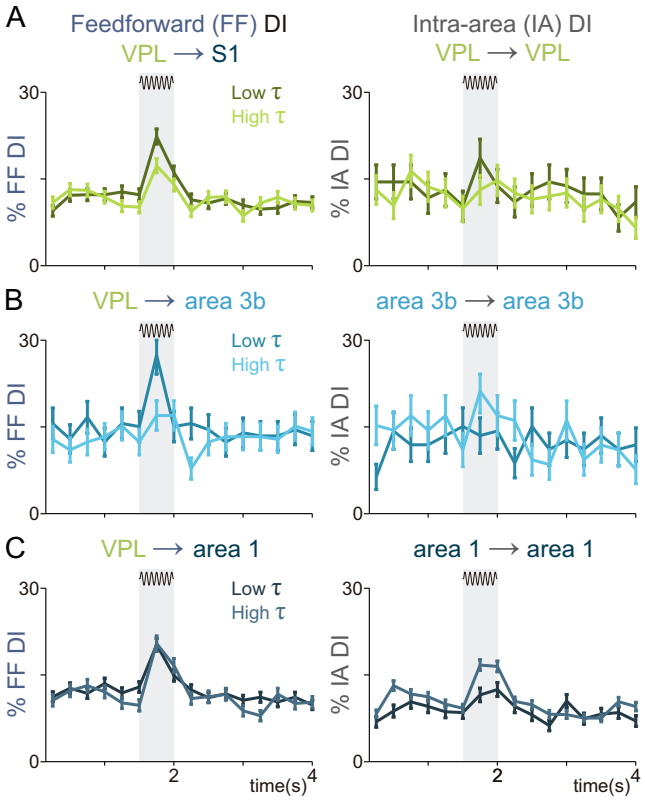


**Figure 6: Feedforward and intra-area interactions show different associations with intrinsic timescales.** Percentage of feedforward information (left) and intra-area unidirectional information (right) in each area during the task for two groups of neurons (low [dark-colored] and high [light] intrinsic timescale neurons). Error bars denote the SEM and shaded areas highlight the stimulus period (0-0.5 s). (A) Left: Percentage of overall outgoing feedforward information from VPL. Right: Percentage of intra-VPL unidirectional DI. (B) Left: Percentage of incoming feedforward information to area 3b. Right: Percentage of intra-area 3b unidirectional incoming connectivity. (C) Left: Percentage of incoming feedforward information to area 1. Right: Percentage of intra-area 1 unidirectional incoming information.

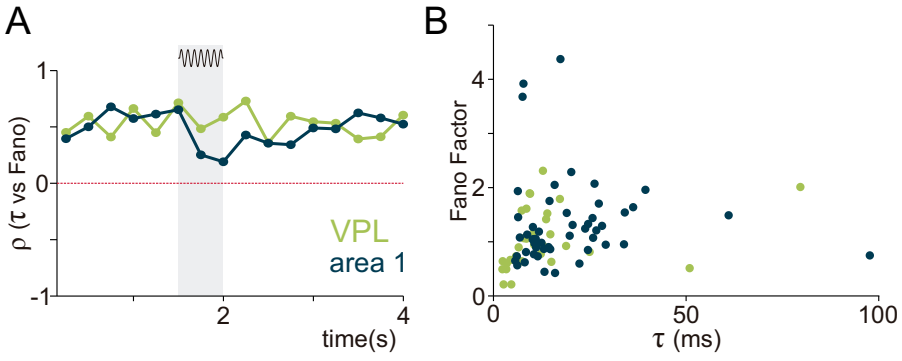


**Figure S1: Timescale and variability correlation in VPL and Area 1.** (A) Spearman's correlation ($\rho$) between the intrinsic timescale and the time-varying Fano factor during the task. In green, $\rho$ across VPL neurons. In dark blue, $\rho$ across area 1 neurons. (B) Scatter plot highlighting the correlation between the intrinsic timescale and the Fano factor during the first half of the stimulus period. Larger correlation for VPL ($\rho$=0.52, n=61) as compared to area 1 ($\rho$=0.21, n=101).

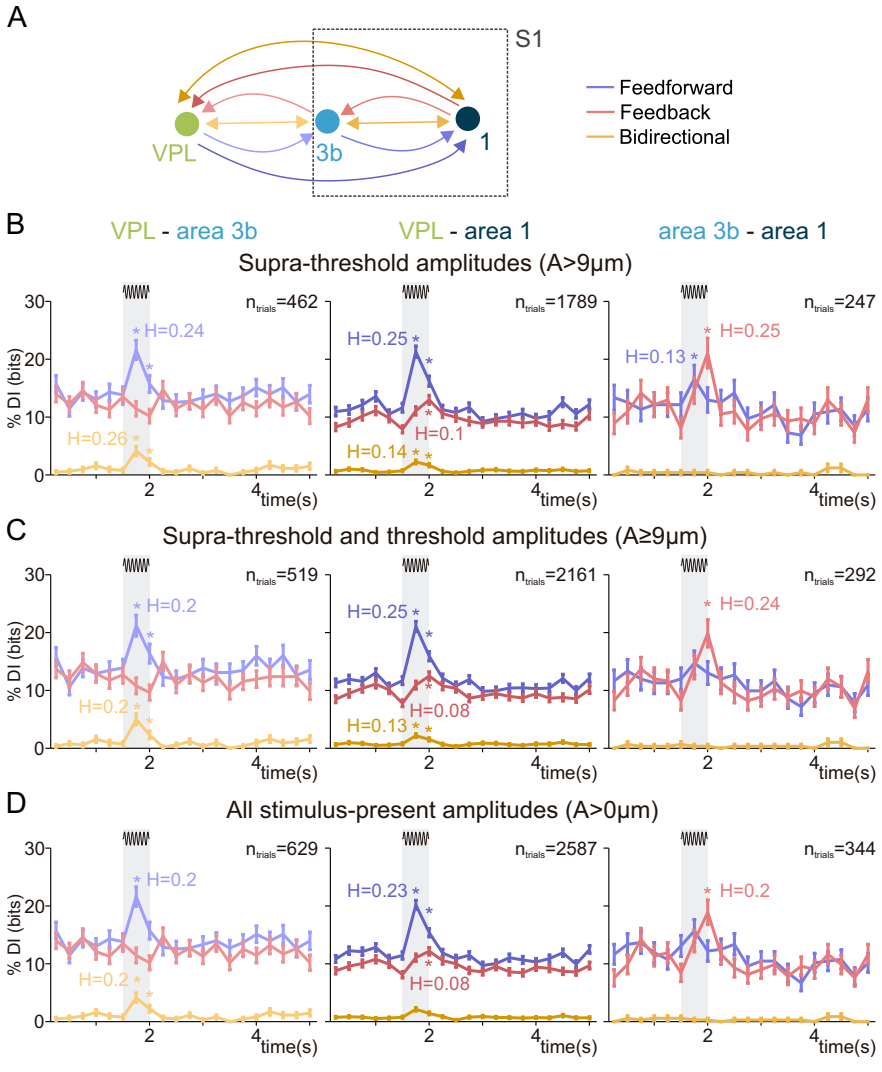


**Figure S2: Inter and intra-area directional interactions in the thalamocortical network based on distinct stimuli groupings.** Reproduction of Fig. 4C as a function of different stimulus amplitude. (A) Scheme showing feedforward and feedback DI and zero-lag synchronization across the areas/subareas VPL, area 3b and area 1 of the somatosensory network. Darker colors represent the same as in Fig. 4. (B) Percentage of feedforward (blue) and feedback (red) DI and zero-lag synchronization (orange) are shown along the task timeline during hits. Results are shown for the area pairs VPL-area 3b (left), VPL-area 1 (middle) and area 3b-area 1 (right). Top: Percentage of DI for supra-threshold amplitudes. Middle: Percentage of DI for supra-threshold and near-threshold amplitudes. Bottom: Percentage of DI for all stimulus-present amplitudes including sub-threshold amplitudes.

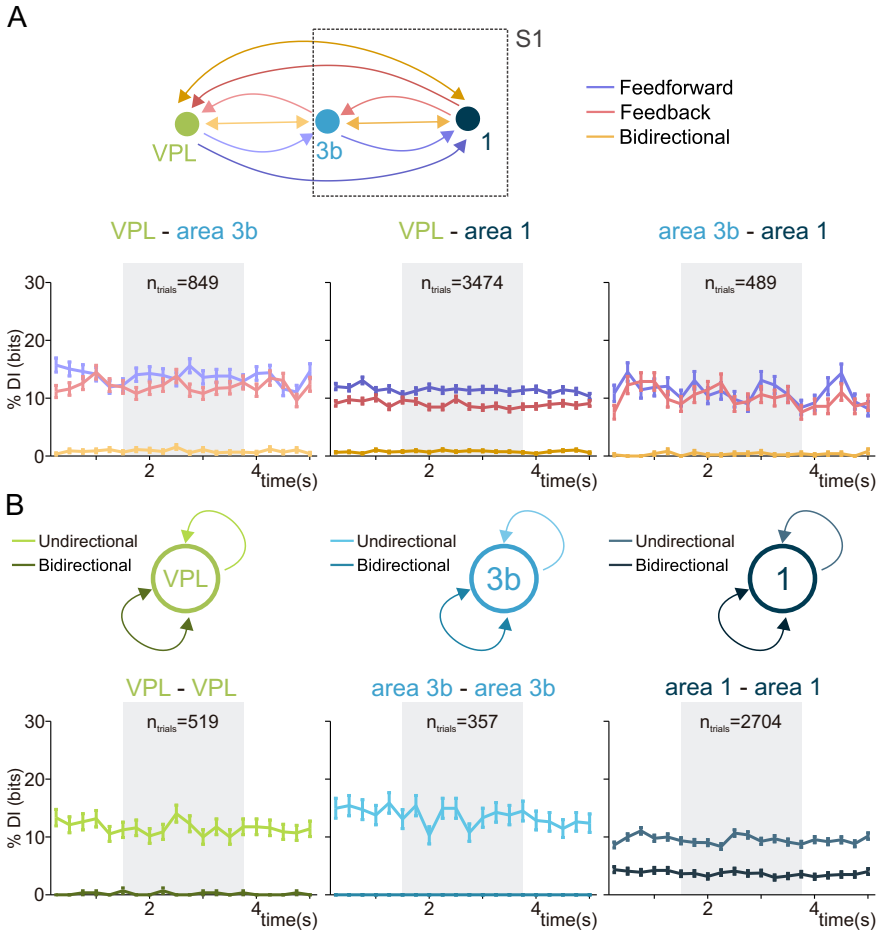


**Figure S3: Inter and intra-area directional interactions in the thalamocortical network during correct rejection (CR) trials.** (A) Scheme showing feedforward, feedback and zero-lag interactions across the areas VPL, 3b and 1 of the somatosensory network. Darker colors same as Fig. 4. (B) Percentage of feedforward (blue) and feedback (red) DI, and zero-lag synchronization (orange) are shown along the task timeline during correct rejections (CR) trials. Left: VPL-area 3b pairs (n=849 trials). Middle: VPL-area 1 pairs (n=3474 trials). Right: area 3b-area 1 pairs (n=349 trials). Error bars denote the SEM. (C) Scheme showing unidirectional and zero-lag interactions within the areas VPL, areas 3b 1. (D) Percentage of DI trials for unidirectional (lighter color) and bidirectional zero-lag interactions (darker color) are shown throughout the task during CR trials. Left: VPL-VPL pairs (n=484 trials). Middle: area 3b-area 3b pairs (n=334 trials). Right: area 1-area 1 pairs (n=2514 trials).

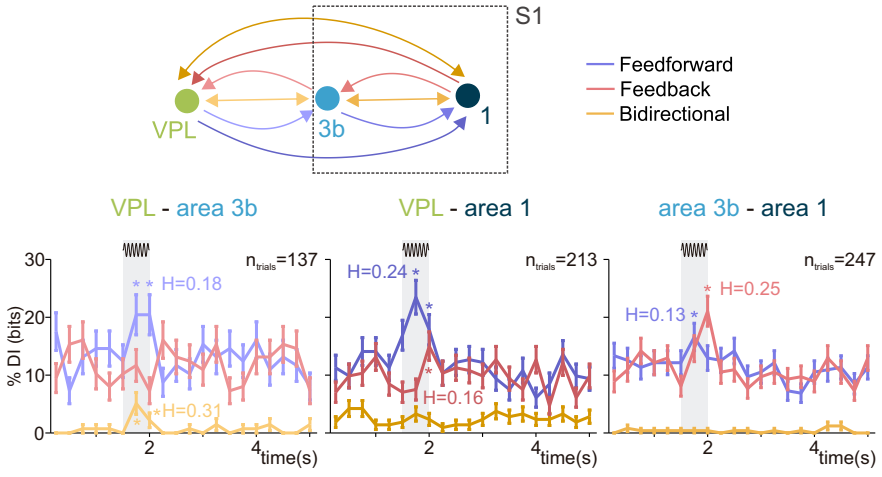


**Figure S4: Inter and intra-area directional interactions in the thalamocortical network during simultaneously recorded trials of area 3b and 1.** Fig 4 particularized for sessions with simultaneous recordings of areas 3b and 1. Percentage of DI trials for feedforward (blue), feedback (red) and bidirectional zero-lag (orange) interactions are shown along the task during supra-threshold hits. Darker colors same as Fig. 4.

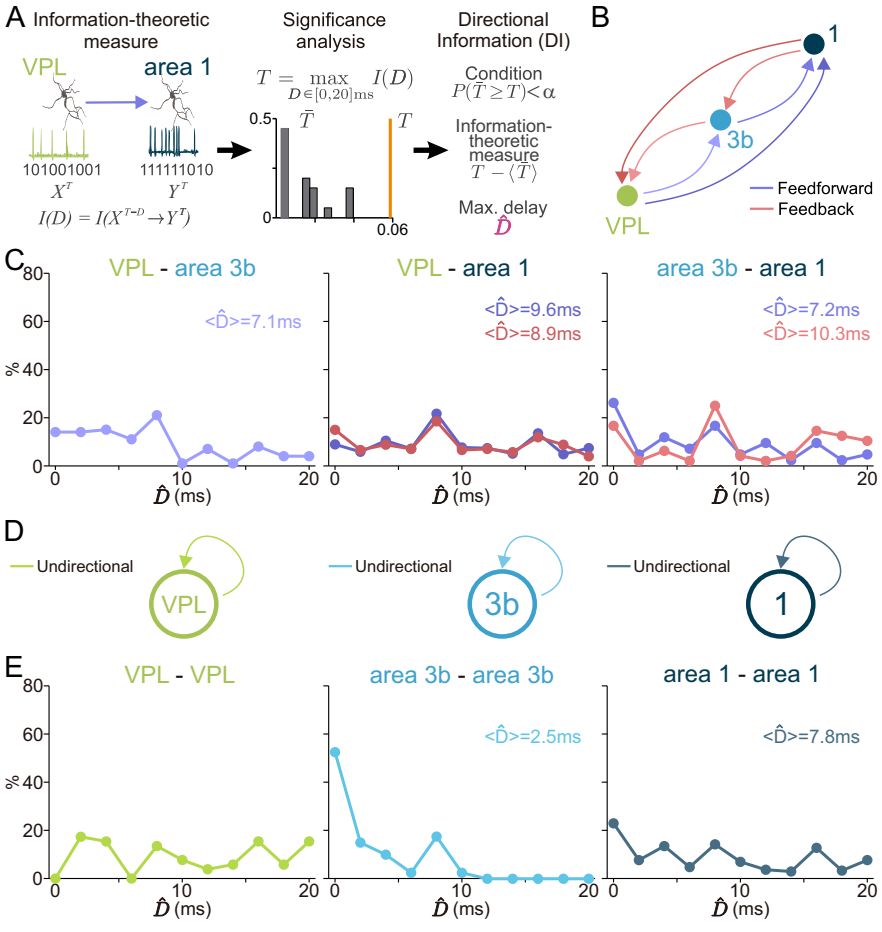


**Figure S5: Inter and intra-area directional interactions delays in the thalamocortical network.** (A), (B) and (D) same as Fig. 4 in structure and color scheme. (C) Histograms of DI delays for the DI types (feedforward and feedback) showing a significant increase (Fig. 4) during the stimulus period. The delays were only selected from the stimulus intervals where the effect was largest. Histograms in percentage and their averages for all tested delays (0:2:20 ms). Left: Delay histogram for VPL-area 3b (n=478 delay values, interval 0-0.25s). Middle: VPL-area 1 (n=1789 delay values; interval 0-0.25s for feedforward, 0.25-0.5s for feedback DI). Right: area 3b-area 1 (n=247 delay values; interval 0.25-0.5s). (E) Histograms of DI delays for the inter-area unidirectional interactions during the interval 0-0.25s of the stimulus period. Left: Delay histogram for VPL-VPL (n=338 delay values). Middle: Delay histogram for area 3b-area 3b (n=216 delay values). Right: area 1- area 1 (n=1606 delay values).